applied sciences

MDPI

Article

Energy Management Strategy for the Hybrid Energy Storage System of Pure Electric Vehicle Considering Traffic Information

Jianjun Hu [1,2,*], Xingyue Jiang [2], Meixia Jia [2] and Yong Zheng [2]

[1] State Key Laboratory of Mechanical Transmission, Chongqing University, Chongqing 400044, China
[2] College of Automotive Engineering, Chongqing University, Chongqing 400044, China; jxy@cqu.edu.cn (X.J.); jiameixia23@163.com (M.J.); zhengyong1992@126.com (Y.Z.)
* Correspondence: hujianjun@cqu.edu.cn; Tel.: +86-139-9607-3282

Received: 8 July 2018; Accepted: 28 July 2018; Published: 31 July 2018

Abstract: The main challenge for the pure electric vehicles (PEVs) with a hybrid energy storage system (HESS), consisting of a battery pack and an ultra-capacitor pack, is to develop a real-time controller that can achieve a significant adaptability to the real road. In this paper, a comprehensive controller considering the traffic information is proposed, which is composed of an adaptive rule-based controller (main controller) and a fuzzy logic controller (auxiliary controller). Through analyzing the dynamic programming (DP) based power allocation of HESS, a general law for the power allocation of HESS is acquired and an adaptive rule-based controller is established. Then, to further enhance the real-time performance of the adaptive rule-based controller, traffic information, which consists of the traffic condition and road grade, is considered, and a novel method combining a K-means clustering algorithm and traffic condition is proposed to predict the future trend of vehicle speed. On the basis of the obtained traffic information, a fuzzy logic controller is constructed to provide the correction for the power allocation in the adaptive rule-based controller. Ultimately, the comparative simulations among the traditional rule-based controller, the adaptive rule-based controller, and the comprehensive controller are conducted, and the results indicate that the proposed adaptive rule-based controller reduces battery life loss by 3.76% and the state of change (SOC) consumption by 3.55% in comparison with the traditional rule-based controller. Furthermore, the comprehensive controller possesses the most excellent performance and reduces the battery life loss by 2.98% and the SOC consumption of the battery by 1.88%, when compared to the adaptive rule-based controller.

Keywords: electric vehicle; hybrid energy storage system; energy management; traffic information

1. Introduction

The consumption of fossil energy and the increasingly rigorous emission standards has led to a widespread concern for pure electric vehicles (PEVs) [1,2]. However, the short lifespan, the low energy, and power density of the energy sources in the PEVs restrict their further application. The hybrid energy storage system (HESS) can deal with these problems by utilizing the large capacity of the battery and the high power of the ultra-capacitor, which contribute to HESS being a popular issue in the research and application area of PEVs [3].

The existence of two energy sources in a HESS brings great flexibility for the control of HESS and an excellent controller can significantly enhance the performance of HESS. The rule-based controller is the most common controller because of its simplicity and convenience, which is mainly classified as the deterministic rule-based controller and the fuzzy logic rule-based controller (which is generally called fuzzy logic controller). The deterministic rule-based controller [4–6] is formulated through defining the

prior thresholds to implement the power allocation of energy sources. Nevertheless, the formulation of thresholds is sensitive to the driving cycles. To reduce the sensitivity of the thresholds to the driving cycles, the fuzzy logic controller [7,8] was put forward to provide a broader rule for the operating of energy sources. However the deterministic and fuzzy rules are essentially the predetermined rules, which greatly rely on the expert experiences. In addition, the filtration based controller was developed in the literature [9,10], according to the filtration principle, which allocates the high frequency of the demand power to the ultra-capacitor and the low frequency to the battery. As all of the controllers above achieve limited economic performance enhancement, numerous optimal algorithms were applied to set up the controllers for HESS. For instance, dynamic programming (DP) [11,12], particle swarm optimization (PSO) [13,14], and convex optimization [15,16] were employed to explore the potential economic performance of HESS. However, these optimal algorithm-based controllers require the information of the driving cycles in advance, which leads to their poor real-time performance. Therefore, to enhance the real-time application of the controllers, the controllers for speed prediction and driving cycle recognition were invented. The model predictive control (MPC) was introduced to predict the future vehicle speed [17–19]. By predicting a period of the future vehicle speed, a mini-global optimal controller is constructed for the period of the driving cycle. Furthermore, some scholars summed up the characteristics of the existing driving cycles and proposed driving cycle recognition-based controllers to improve the adaptability of the controllers to the driving cycles [20,21]. However, the future speed prediction and the driving cycle recognition are completed on the basis of the existing driving cycles, which means that it is difficult to guarantee an accurate prediction and recognition in the real road all of the time. What is more, the high computing load of the MPC and the driving cycle recognition-based controller limits their further application. In all of controllers above, the traffic condition and the road grade were ignored. It can be observed in the literature [22,23] that the road grade plays a critical role in influencing the power allocation of the controllers. Through establishing the controller considering the road grade, the situation that the controllers deal with is much closer to the real road, so the real-time performance of controllers is further enhanced. Also, the traffic condition is not negligible in the real driving. In the literature [24], a predictive controller adopting the Monte Carlo approach is proposed, so as to handle the information of the traffic condition. In general, most of the research for the control of HESS does not consider the impact of the traffic information on the power allocation. Moreover, in these controllers ignoring the traffic information, some problems, such as the adaptability to driving cycles or computing load, restrict their application to the real road, and in those controllers considering traffic information, the road grade, the traffic condition and the vehicle speed are not taken into account at the same time in a controller. Furthermore, the power allocations of these controllers are mainly determined by the principle of the traditional controllers, which contributes to their poor adaptability to the driving cycles.

Therefore, in order to enhance the adaptability of the traditional controllers to the driving cycles, an adaptive rule-based controller is proposed in this paper to get rid of the reliance on the expert experiences through analyzing the general law of the optimal power allocation of HESS under various driving cycles. Because of the uncertain accuracy of the vehicle speed prediction, the future trend of the vehicle speed is selected to be handled. Then, a fuzzy logic controller considering the traffic condition, the road grade, and the future trend of the vehicle speed is established. By combining the adaptive rule-based controller and the fuzzy logic controller, a comprehensive controller is constructed.

The rest of this paper is organized as follows. Section 2 gives the basic parameters and the battery model. The formulation of an adaptive rule-based controller is illustrated in Section 3. Section 4 demonstrates the fuzzy logic controller considering the traffic information. Comparative simulations and the results analysis are conducted in Section 5. Section 6 discusses the conclusions of this paper.

2. Parameters and Model

In this paper, a semi-active HESS with direct current (DC)/DC and ultra-capacitor connection is selected by weighing the cost, efficiency, and control difficulty of the various structures of HESS [25], as described in Figure 1. Table 1 lists the basic parameters of the electric vehicle.

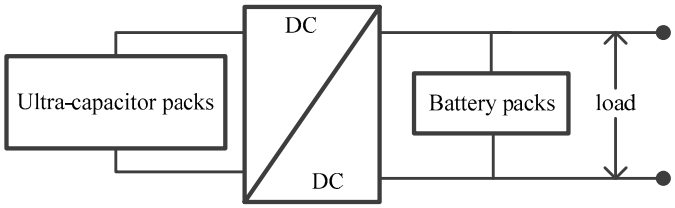

Figure 1. Semi-active structure with direct current (DC)/DC and ultra-capacitor connection.

Table 1. Basic parameters of vehicle.

Parameter	Value
Total weight/kg	1900
Curb weight/kg	1500
Front section/m^2	2.3
Aerodynamic drag factor	0.29
Rolling resistance	0.012
Wheel radius/m	0.307
Motor rated power/kW	80
Motor peak power/kW	105
Motor voltage class/V	≤360

This paper chooses a lithium iron phosphate battery and its basic parameters are listed in Table 2. Battery life is one of the most crucial indexes for the economic performance of HESS. In order to evaluate the battery life, it is essential to set up an accurate capacity loss model of the battery.

Table 2. Basic parameters of a lithium iron phosphate battery.

Index	Value
Nominal capacity/Ah	20
Nominal voltage/V	3.2
Internal resistance/mΩ	≤6
Weight/g	514 ± 10
Charge voltage/V	3.65 ± 0.05
Discharge termination voltage/V	2.0
Operating temperature/°C	−20 ~60

Referring to the semi empirical model of capacity loss for a lithium iron phosphate battery in the literature [26], and the modified semi empirical model [27,28], the capacity loss model of a lithium iron phosphate battery is established, as illustrated in Equation (1), where operating temperature, the influences of the battery discharge rate, the battery discharge depth, and the discharge time on the capacity loss of battery are taken into account.

$$Q_{loss} = B_1 e^{\frac{-31329.7}{RT}} \times \left(\sqrt[0.55]{(1.169e^{-0.3375n} + 0.146e^{0.1271n}) \times e^{(-0.1494+0.1494n)}} \times A_{hn} \right)^{0.55} \quad (1)$$

where Q_{loss} represents the capacity loss of the battery, R denotes the ideal gas constant, and T is the Kelvin temperature of the battery operating, K. A_{hn} is the Ah-throughput, Ah. n presents the charge rate and B_1 is the pre-exponential factor.

Generally, it is considered that the battery life is terminated when the battery capacity reaches 20% of its nominal capacity. The life loss of battery, L_{loss}, is indicated in Equation (2).

$$L_{loss} = \frac{A_{hn}}{A_{hn(20\%)}} \tag{2}$$

where $A_{hn(20\%)}$ represents the Ah-throughput when the battery capacity arrives at 20% of its nominal capacity.

3. Adaptive Rule Based Controller

As a global optimal algorithm, DP can achieve the theoretical optimal performance of HESS under a certain driving cycle. This paper selects DP to implement the offline optimization for the instantaneous power allocation of HESS under various types of driving cycles, and according to the offline data, a general law of instantaneous power allocation is discovered and an adaptive rule-based controller is established.

3.1. Offline Optimization of Dynamic Programming

In the DP-based controller, the control variable is the power of the battery, P_{bat}, which is depicted in Equation (3), and the SOC of the battery, SOC_{bat}, and the ultra-capacitor, SOC_{uc}, are selected as the state variables, as shown in Equation (4).

$$u = \{P_{bat}(t)\} \tag{3}$$

$$x = \{SOC_{bat}, SOC_{uc}\} \tag{4}$$

The discretization step of the optimization dt is 1 s and the state transition can be calculated by Equations (5) and (6).

$$SOC_{bat}(k+1) = SOC_{bat}(k) - \frac{\left(U_{bat} - \sqrt{U_{bat}^2 - 4R_{bat}P_{bat}(k)}\right)dt}{2R_{bat}Q_{rate}\cdot 3600} \tag{5}$$

$$SOC_{uc}(k+1) = SOC_{uc}(k) - \frac{\left(U_{uc} - \sqrt{U_{uc}^2 - 4R_{uc}P_{uc}(k)}\right)dt}{2R_{uc}C(U_{uc\_max} - U_{uc\_min})} \tag{6}$$

where U_{bat} and R_{bat} represent the voltage and the resistance of the battery, respectively. Similarly, the voltage, resistance, and power of the ultra-capacitor are labeled by U_{uc}, R_{uc}, and P_{uc}, respectively. C presents the capacity loss of the battery. U_{uc_max} and U_{uc_min} denote the maximum and minimum of the ultra-capacitor voltage.

The indexes that greatly reflect the economic performance of HESS are the life and the electricity consumption of the battery. Therefore, in this paper, the capacity loss of the battery, C, and the electricity depletion of the battery, ΔSOC, which are depicted in Equations (7) and (8), are selected as the control objectives.

$$C = \frac{I_{bat}}{Q_{rate}} \tag{7}$$

$$\Delta SOC = \frac{I_{bat} \times dt}{3600 Q_{rate}} \tag{8}$$

Actually, in a certain state, the discrete step, dt, and the nominal capacity of battery, Q_{rate}, are determined. Thus, the optimal decision of the DP is the same when Equation (7) or Equation (8) is selected to be the cost function. In this paper, the cost function J is computed by the following:

$$J = \sum_{k=0}^{N-1} \frac{I_{bat}}{Q_{rate}} \tag{9}$$

3.2. Formulation of Adaptive Rule Based Controller

The DP-based controller is applied to UKBUS6, MANHATTN, NYCC, UDDS, New York Bus, INDIAHWY, EUDC_LOW, and HWFET driving cycles. Urban, suburban, and expressway conditions are included in these driving cycles. In the offline optimization of DP under various driving cycles, the relationship between the output power of the ultra-capacitor and the demand power of the motor can be divided into three regions, except for the UDDS driving cycle, as described in Figure 2. In each region, an approximate linear relationship exists between the output power of the ultra-capacitor and the demand power of the motor. It can be seen from region 1, that when the demand power of the motor is negative (the vehicle is braking), the ultra-capacitor absorbs all of the braking energy. Because of the efficiency of the DC/DC converter, the power of the ultra-capacitor is slightly less than the motor power, and the slope of the linear relationship is less than 1. Region 2 indicates that the ultra-capacitor will not provide the output power when the demand power of the motor is positive and lower than a certain threshold. Under the low demand power of the motor, it is relatively safe for the battery to discharge alone, and the addition of ultra-capacitor, it will reduce the system efficiency of HESS. In region 3, when the demand power of the motor is greater than a threshold, both the battery and ultra-capacitor provide the output power, and the output power of the ultra-capacitor linearly increases with the demand power of the motor. As for the UDDS driving cycle, there is an extra region, region 4. At a few or more seconds after many time points in region 4, a higher demand of power is required and the DP, which is a global optimal algorithm, allocates the electricity of the ultra-capacitor to these points, demanding greater power. Because of the limited electricity of the ultra-capacitor, the time points in region 4 receive relatively low power.

As a result of the obvious regularity of the optimal instantaneous power allocation, the average positive power of the various driving cycles and the thresholds of the demand power of the motor in region 2 are counted. Also, the linear relationship in region 3 is fitted and region 4 of the UDDS is ignored because of the individual phenomenon. The results are listed in Table 3.

Table 3. Data statistics of each driving cycle.

Driving Cycle	Average Positive Power/kW	Threshold in Region 2/kW	Fitting Curves in Region 3
UKBUS6	3.360	3.291	$f(x) = 0.7647x - 3.040$
MANHATTAN	6.172	5.132	$f(x) = 0.7850x - 4.366$
NYCC	7.121	6.673	$f(x) = 0.7855x - 5.905$
UDDS	10.202	6.486	$f(x) = 0.7772x - 6.187$
New York Bus	11.000	8.070	$f(x) = 0.7767x - 7.065$
INDIAHWY	11.669	10.85	$f(x) = 0.7892x - 8.444$
EUDC_LOW	11.770	13.68	$f(x) = 0.7872x - 11.15$
HWFET	14.251	18.67	$f(x) = 0.7628x - 14.53$

From Table 3, the thresholds in region 2 increase with the average positive power under the various driving cycles. The linear relationship in region 3 between the output power of the ultra-capacitor and the demand power of the motor can be expressed by $f(x) = ax + b$. The slope, a, of each driving cycle is close to the others, which is supposed to around 0.7785 and the values of b increase with the average positive power of the driving cycle. Thus, by means of the linear fitting of both the relationship between the thresholds in region 2 and the average positive power, and the relationship between the value of b and the average positive power, the threshold of the demand power of the motor and the linear curves in region 3 can be obtained if the average positive power is received.

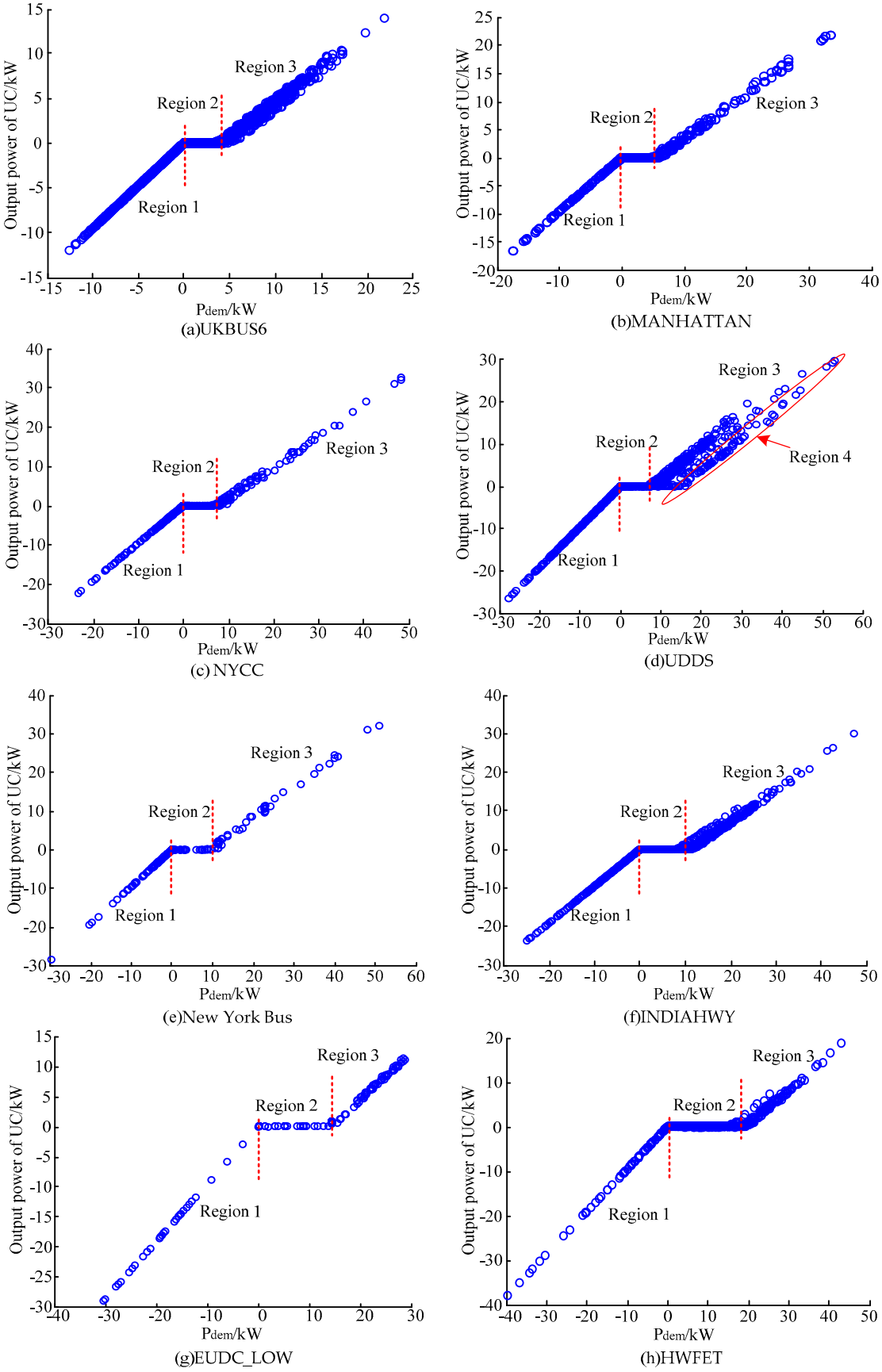

Figure 2. Power allocation under different driving cycles. *UC*—ultra-capacitor; P_{dem}—demand power of motor.

In the real driving, the driving condition possesses continuity and its historical information can be employed to evaluate the current driving condition. In this paper, the historical information of the driving condition from the current time to 100 s is selected, in order to obtain the average positive power. Through the data analysis and handling above, the relationship between the output power of the ultra-capacitor and the demand power of the motor is acquired, according to the average positive power of the driving condition. Thus, according to the rule-based controller [29], the adaptive rule-based controller is formulated, as illustrated in Table 4.

Table 4. Adaptive rule-based controller. SOC—state of change; UC—ultra-capacitor.

Operating Condition	Switch Condition	Power Allocation
Driving: battery and UC	$P_{min} < P_{dem}$ and $SOC_{uc,min} < SOC_{uc}$	$P_{uc} = aP_{dem} + b$ $P_{bat} = P_{dem} - P_{uc}$
Driving: battery	$P_{min} \leq P_{dem}$ and $SOC_{uc} \leq SOC_{uc,min}$	$P_{bat} = P_{dem}$ $P_{uc} = 0$
Driving: battery	$0 \leq P_{dem} \leq P_{min}$	$P_{bat} = P_{dem}$ $P_{uc} = 0$
Braking: UC	$P_{dem} < 0$ and $SOC_{uc} < SOC_{uc,max}$	$P_{uc} = P_{dem}$ $P_{bat} = 0$
Braking: neither of them	$P_{dem} < 0$ and $SOC_{uc,max} \leq SOC_{uc}$	$P_{bat} = 0$ $P_{uc} = 0$

4. Comprehensive Controller Considering Traffic Information

In the real driving, it is inevitable to encounter the traffic congestion, upgrade or downgrade, and traffic lights, which are the main elements of traffic information. In these elements, the traffic condition and the road grade significantly affect the demand power of the motor. Thus, to further enhance the performance of the controllers, the traffic condition and the road grade should be taken into account. At present, the global positioning system (GPS) and geographic information system (GIS) are applied to the vehicle [30], which makes it feasible to design the controllers considering traffic information. In this section, the access to the traffic condition and the road grade are discussed. Moreover, to predict the future trend of vehicle speed, a novel method is proposed and a fuzzy logic controller considering the traffic condition is constructed.

4.1. Access to the Traffic Condition and the Road Grade

The World Light Test Procedure (WLTP) driving cycle is chosen as a test driving cycle and the information of the traffic condition and the road grade is added into the WLTP driving cycle [31].

After the driver sets the driving route, the real-time traffic condition can be obtained by means of the vehicle navigation map. Take Google maps as an example, the real-time traffic condition will be displayed after setting the driving route. Red represents traffic congestion and the average vehicle speed is less than 10 km/h. The moderate traffic fluency is denoted by yellow and the average vehicle speed is at 10 ~40 km/h. Green presents a good traffic condition and the average vehicle speed is greater than 40 km/h. According to Google maps, the traffic condition of the WLTP driving cycle is shown in Figure 3.

Similarly, GIS can provide the altitude of the real road and the road grade, i, can be calculated by Equation (10). The diagram of the road grade calculation is depicted in Figure 4.

$$i = \tan\left(\sin^{-1}\frac{A_2 - A_1}{L}\right) \times 100\% \tag{10}$$

where A_1 is the altitude of the current position of the vehicle, and A_2 is the altitude of the next sampling point. L represents the driving distance between the current position of the vehicle and the sampling point.

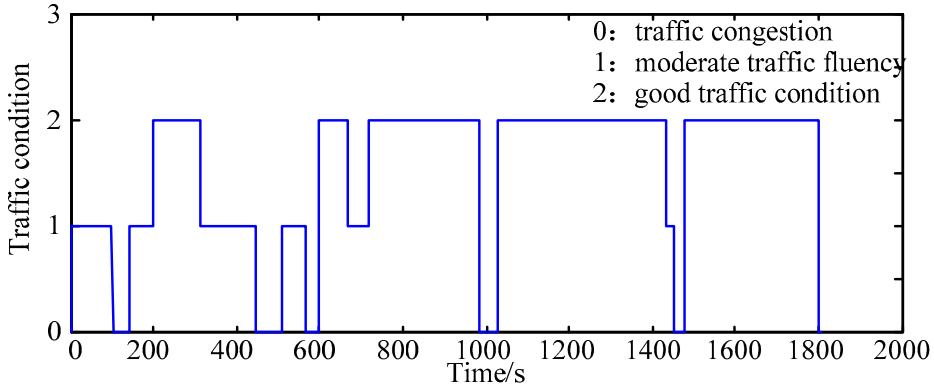

Figure 3. Traffic condition of the World Light Test Procedure (WLTP) driving cycle.

During the process of adding the road grade into the WLTP driving cycle, the road grade, the vehicle speed, and the length of the slope should follow the relevant rules [31]. Figure 5 describes the added information of the road grade in the WLTP driving cycle.

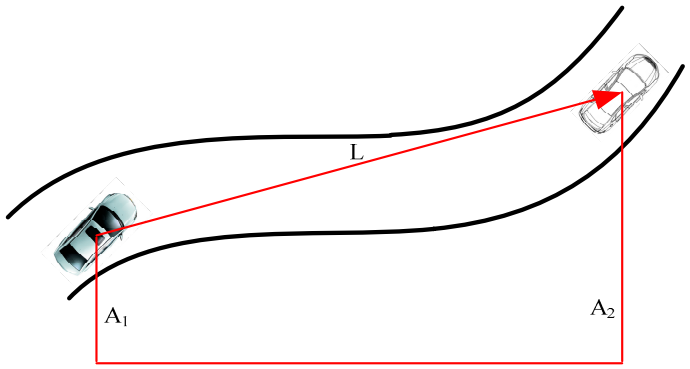

Figure 4. Diagram of road grade calculation.

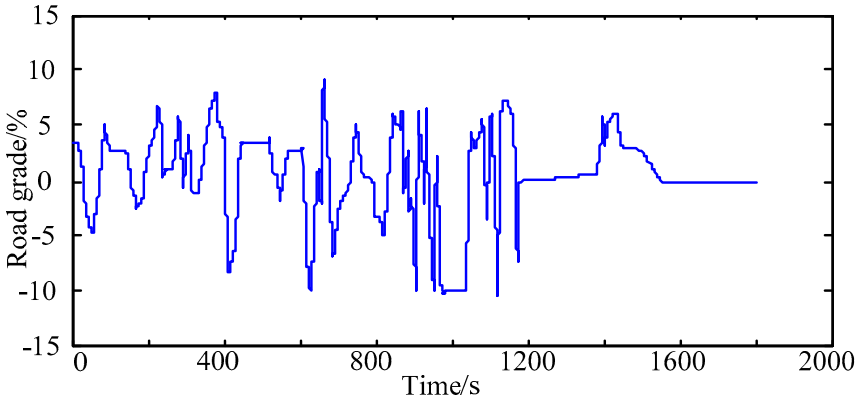

Figure 5. Added information of road grade in WLTP driving cycle.

4.2. Future Trend Prediction of Vehicle Speed

The instantaneous power allocation in the traditional controller is decided by the current demand power of the motor. However, the limited quantity of the electricity of the ultra-capacitor cannot always meet the energy and power requirement from the controller. To better develop the effect of the controller, it is necessary to predict the future trend of the vehicle speed and to guarantee that the electricity of the ultra-capacitor is in a proper range. This section employs the K-means clustering

algorithm to implement the future trend prediction of the vehicle speed, and the prediction process is as follows:

① The combined driving cycle, including MANHATTAN, NYCC, UDDS, NEDC, WVUINTER, and HWFET, is selected as the sample driving cycle, as shown in Figure 6. These six driving cycles cover urban, suburban, and expressway condition.

② The sampling period is 1 s and the driving cycle between the two sampling points is a driving cycle block. The average accelerated speed, the standard deviation of the vehicle speed, and the difference between the initial speed and the last speed of a driving cycle block are selected as the characteristic parameters of the driving cycles [32]. The characteristic parameters of 10 s are calculated at each sampling point.

③ Referring to the K-means clustering algorithm [33], three cluster centers are obtained, which are the cluster centers of the speed descending c_1, speed stabling c_2, and speed rising c_3, as Table 5 lists.

④ After obtaining the cluster centers, the distance, d_j, from various characteristic parameters to the jth cluster center can be computed by Equation (11). If $d_1 < d_2$ & $d_2 < d_3$, the state of the vehicle speed is the type of speed descending, and the state of the vehicle speed belongs to the speed stabling when $d_2 < d_1$ & $d_2 < d_3$. If $d_3 < d_1$ & $d_3 < d_2$, the vehicle speed is considered to be a speed rising.

$$d_j = \sqrt{(x_1 - c_{j1})^2 + (x_1 - c_{j2})^2 + (x_1 - c_{j3})^2} \tag{11}$$

where j can be 1, 2, or 3. c_{j1} denotes the value of the average accelerated speed in the jth cluster. The standard deviation of the vehicle speed is labeled by c_{j2}, and c_{j3} represents the difference between the initial speed and the last speed of a driving cycle block.

The state of the vehicle speed under the WLTP driving cycle is displayed in Figure 7.

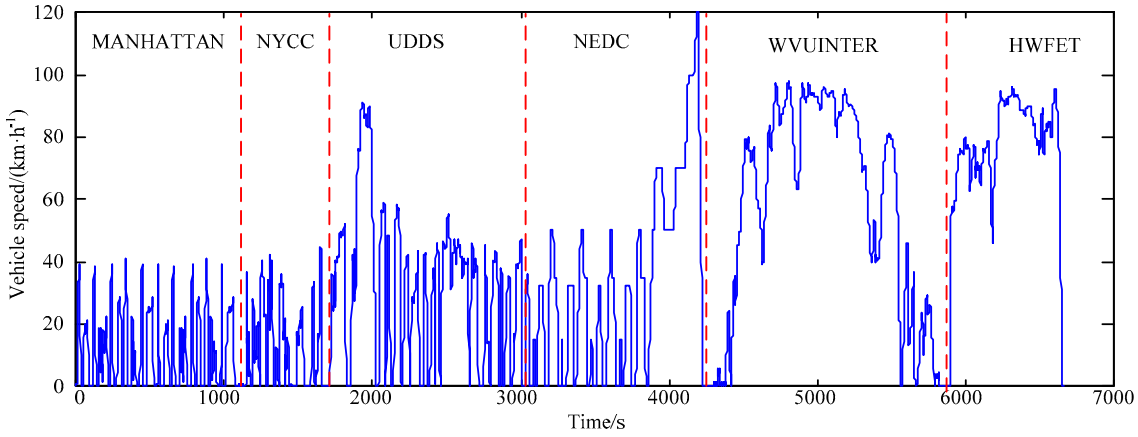

Figure 6. Sample driving cycle.

Table 5. Three cluster centers.

Cluster Centers	c_1	c_2	c_3
Average accelerated speed	−0.65394301496	−0.00551733775	0.51745111141
Standard deviation of vehicle speed	7.78720463753	1.10825192133	6.05417011930
Speed difference	−22.1134815365	−0.1531105304	17.3566038619

Speed difference represents the difference between the initial speed and the last speed of a driving cycle block.

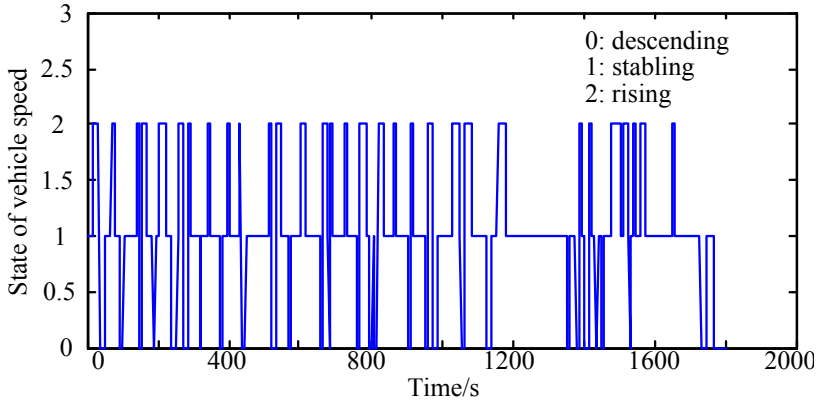

Figure 7. State of vehicle speed under a WLTP driving cycle.

The traffic condition is combined with the state of the vehicle speed, in order to better predict the future trend of the vehicle speed.

If the vehicle speed belongs to the speed stabling, the vehicle speed is considered to be steady, no matter traffic condition.

If the vehicle speed is the type of speed descending, it is considered that when the traffic condition is congested, modestly fluent, and fluent, and the future trend of the vehicle speed is considered to descend largely, moderately, and slightly, respectively, in a short time.

If the vehicle speed is the type of speed rising, the future trend of the vehicle speed is considered to rise largely, moderately, and slightly when the traffic condition is congested, moderately fluent, and fluent, respectively.

4.3. Optimization of Instantaneous Power Allocation

The future trend of the vehicle speed is obtained in Section 4.2 and the information of the road grade can be acquired by GIS. It should be noted that the grade of the front road of 50 m is regarded as the input for the controller. A fuzzy logic controller is designed to correct the output power allocation of the ultra-capacitor. In the controller, the demand power of the motor, P_{dem}, the future trend of the vehicle speed, v_{trend}, and the future road grade, G_{road}, are chosen to be the input variables of the fuzzy logic controller, and the output variable is the correction coefficient of the output power of the ultra-capacitor, α_{uc_corr}. The concrete definition of the controller is listed in Table 6.

Table 6. Input and output variables definition of fuzzy controller.

Input and Output	Actual Domain	Fuzzy Domain	Membership Function	Fuzzy Subset Levels
P_{dem}	0 ~ 70	0 ~ 1	Gauss type/Bilateral Gauss	3
v_{trend}	−3 ~ 3	−3 ~ 3	Triangle	7
G_{road}	−10 ~ 10	−1 ~ 1	Triangle	7
α_{uc_corr}	−0.2 ~ 0.2	−0.2 ~ 0.2	Gauss type/Bilateral Gauss	7

When P_{dem} is middle, if v_{trend} is rising and G_{road} becomes larger, α_{uc_corr} should be increased. α_{uc_corr} is decreased if v_{trend} is descending and G_{road} becomes smaller.

When P_{dem} is small, α_{uc_corr} should be increased if v_{trend} is rising and G_{road} becomes larger. In the rest of the cases, α_{uc_corr} is reduced.

When P_{dem} is large, if v_{trend} is greatly descending and G_{road} becomes very smaller, α_{uc_corr} is decreased. Under the remain circumstances, α_{uc_corr} is increased.

The idea of the fuzzy logic controller is as follows, as described in Figure 8.

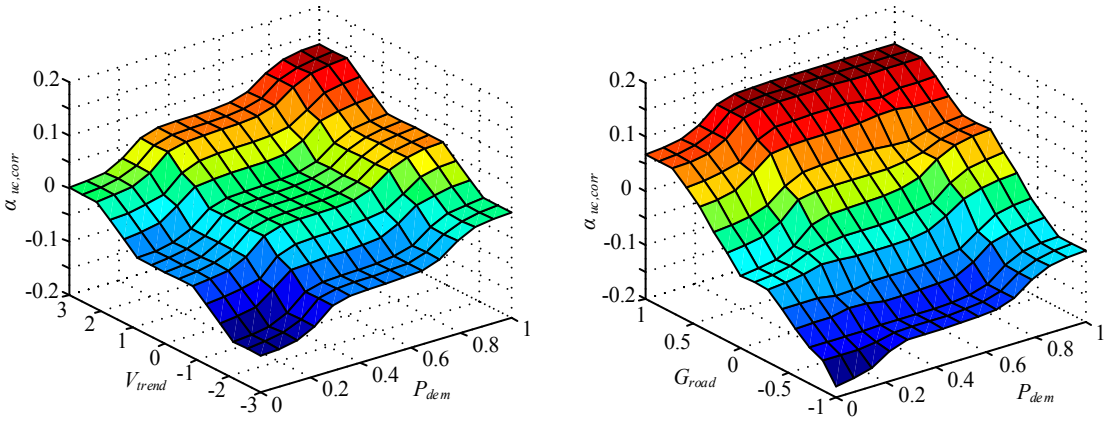

Figure 8. Diagram of fuzzy logic controller.

Obviously, the traffic information cannot be obtained everywhere and every time. Thus, a comprehensive controller is established, as Figure 9 illustrates. If the traffic information cannot be acquired, the adaptive rule-based controller proposed in Section 2 is selected as the unique controller, and the final coefficient of the output power allocation of the ultra-capacitor α_{uc_final} is equal to α_{uc_adap}. If the traffic information is received, the adaptive rule-based controller is regarded as the main controller, and the fuzzy logic controller is chosen as the auxiliary controller. The final coefficient of the output power allocation of the ultra-capacitor α_{uc_final} is equal to the sum of α_{uc_adap} and α_{uc_corr}.

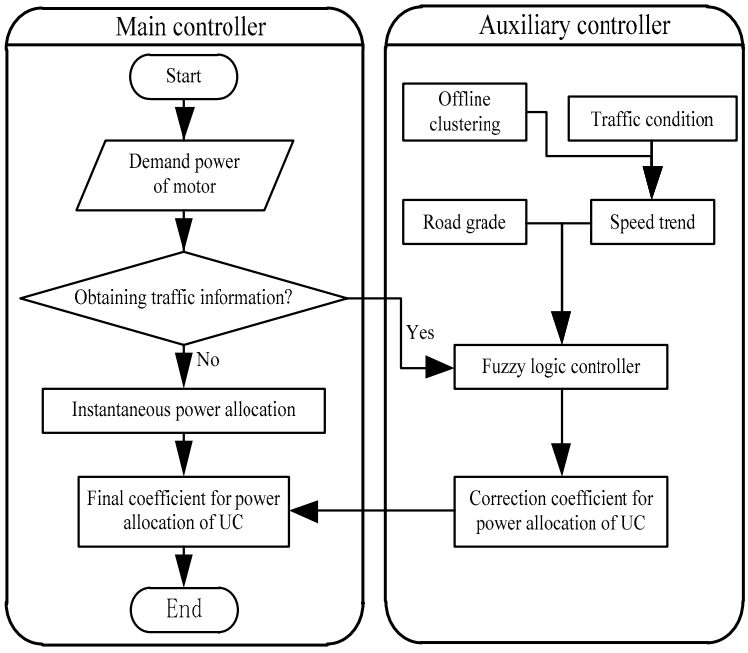

Figure 9. Comprehensive controller considering traffic information.

5. Results

Comparative simulations among the traditional rule-based controller, adaptive rule-based controller, and comprehensive controller considering the traffic information are conducted under the WLTP driving cycle. The traditional rule-based controller is illustrated in Table 7, which possesses a superior economic performance in comparison to other traditional controllers [10]. P_{min} is the threshold of the output power of the battery.

Table 7. Traditional rule-based controller.

Operating Conditions	Switch Requirement	Power Allocation
Battery discharges alone	$P_{min} \leq P_{dem}$ & $SOC_{uc} \leq SOC_{uc,min}$	$P_{bat} = P_{dem}$, $P_{uc} = 0$
Battery discharges alone	$0 \leq P_{dem} < P_{min}$ & $SOC_{uc,tag} \leq SOC_{uc}$	$P_{bat} = P_{dem}$, $P_{uc} = 0$
Battery and UC discharge	$P_{min} \leq P_{dem}$ & $SOC_{uc,min} < SOC_{uc}$	$P_{bat} = P_{min}$, $P_{uc} = P_{dem}$-P_{min}
Battery discharges and UC charges	$0 \leq P_{dem} < P_{min}$ & $SOC_{uc} < SOC_{uc,tag}$	$P_{bat} = P_{dem} + P_{ch}$, $P_{uc} = -P_{ch}$
UC absorbs braking energy	$P_{dem} < 0$ & $SOC_{uc} < SOC_{uc,max}$	$P_{bat} = 0$, $P_{uc} = P_{dem}$
Neither of them absorbs the braking energy	$P_{dem} < 0$ & $SOC_{uc,max} \leq SOC_{uc}$	$P_{bat} = 0$, $P_{uc} = 0$

At the termination of the driving cycle, to prevent the comparison error caused by the unequal SOC of the ultra-capacitor in the three controllers, the battery compensates the SOC of the ultra-capacitor to the same standard, as depicted in Equation (12).

$$\Delta SOC_{bat} = \frac{\Delta SOC_{uc} \times E_{uc} \times \eta}{SOC_{uc.max} \times U_{bat} \times Q_{rate}} \tag{12}$$

where, ΔSOC_{bat} denotes the SOC that battery compensates the ultra-capacitor. ΔSOC_{uc} presents the difference value of the final SOC to the initial SOC. E_{uc} represents the total energy of the ultra-capacitor. η is the efficiency of the DC/DC converter and U_{bat} is the voltage of the battery.

The simulation results of the battery SOC and life loss are listed in Table 8. Table 9 illustrates the use of the battery in the three controllers. The details of the simulation results are given in Figures 10–13. It is not hard to discover, from Table 9, that the battery in the traditional rule-based controller possess the most using times and the highest average power, which leads to the great life loss of battery and the large consumption of SOC. As Figures 10 and 11 depict, due to the fixed rules, the traditional rule-based controller cannot adjust its power allocation according to the driving cycle so that its ultra-capacitor always maintains high quantity of electricity. Actually, when the demand power is low, in order to reduce the use of the battery, the ultra-capacitor can consume its electricity and regain energy through regenerative braking. Thus, the adaptive rule-based controller and the comprehensive controller increase the use of the ultra-capacitor by judging the current driving condition and utilizing the general law of optimal power allocation. Moreover, the high electricity constricts of the ultra-capacitor in the traditional rule-based controller ensures that the battery frequently charges the ultra-capacitor, which further increases the battery using times. The frequent electricity transferring from the battery to the ultra-capacitor is detrimental to the system efficiency. It can be observed in Table 8 that compared to the traditional rule-based controller, the adaptive rule-based controller reduces the battery life loss by 3.76% and the SOC consumption by 3.55% by properly using the ultra-capacitor. However, because of the lack of traffic information, the adaptive rule-based controller fails to achieve a further adjustment for the power allocation. In contrast, through the acquirement of the traffic condition and road grade, the comprehensive controller applies the electricity of the ultra-capacitor to the time points with a great power demand, which means that, as described in Figure 12, at many times, the comprehensive controller achieves the lower output power of the battery in comparison with the adaptive rule-based controller. Therefore, as can be seen from Table 8, compared to the adaptive rule-based controller, the comprehensive controller reduces the battery life loss by 2.98% and the SOC consumption of battery by 1.88%.

Table 8. SOC and life loss of battery.

Controllers\Battery Index	$SOC_{batt\_initial}$ [1]	SOC_{batt_final} [2]	Battery Life Loss
TRBC [3]	0.9	0.7788	1.4028×10^{-4}
ARBC [4]	0.9	0.7831	1.3501×10^{-4}
CC [5]	0.9	0.7853	1.3106×10^{-4}

[1] initial SOC of battery; [2] final SOC of battery; [3] traditional rule-based controller; [4] adaptive rule-based controller; [5] comprehensive controller.

Table 9. Results of battery in three controllers.

Battery index\Controllers	TRBC	ARBC	CC
Battery using times	13,074	10,933	9564
Average power of battery/kW	9.31	9.05	8.87

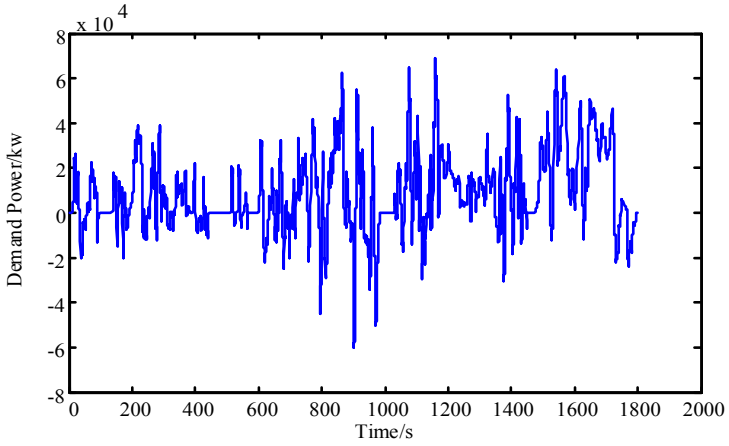

Figure 10. Demand power of WLTP driving cycle.

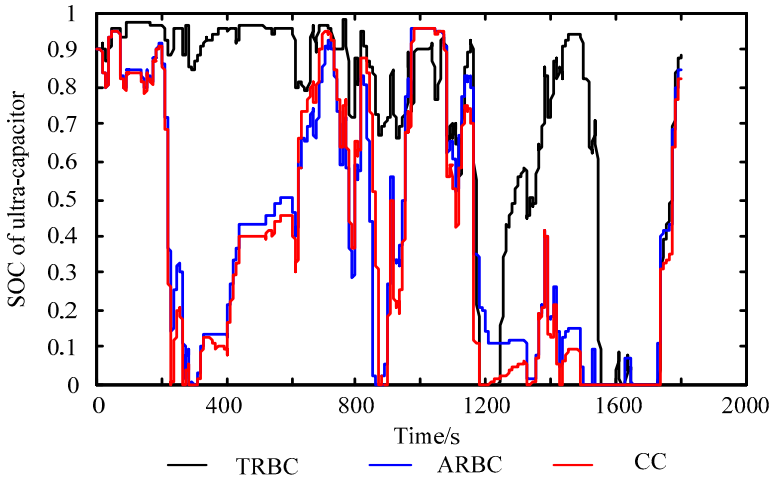

Figure 11. State of change (SOC) of the ultra-capacitor.

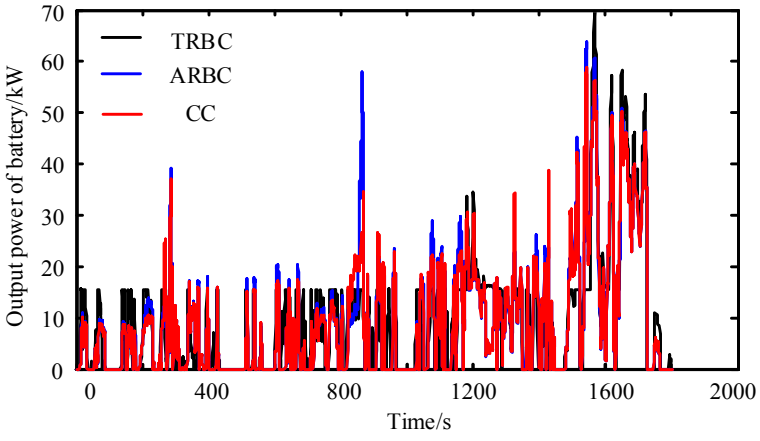

Figure 12. Output power of battery.

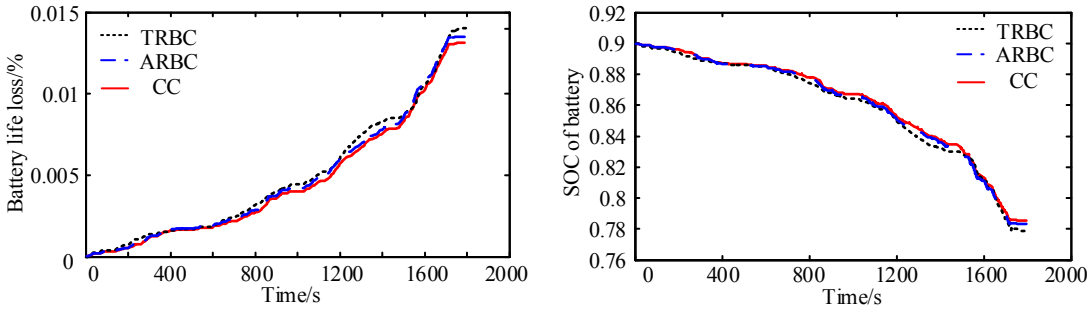

Figure 13. Life loss and SOC of battery.

6. Conclusions

To better implement the power allocation of HESS, this study conducts the offline optimization for the power allocation of HESS by means of DP and through the analysis of offline data from DP, and a general law of the power allocation of HESS is discovered. On the basis of the law, an adaptive rule-based controller is proposed. Then, to further enhance the real-time performance of the controller, the traffic information, including traffic condition and road grade, is taken into account. Moreover, the future trend prediction of vehicle speed is obtained by combining a K-means clustering algorithm and the traffic condition. By comprehensively considering the traffic information and the future trend of vehicle speed, a fuzzy logic controller is developed to correct the coefficient of power allocation in the adaptive rule-based controller. Thus, a comprehensive controller is established by selecting the adaptive rule-based controller as the main controller and the fuzzy logic controller as the auxiliary controller. In conclusion, the following key findings are acquired:

(1) A general law exists in the optimal power allocation of HESS under various types of driving cycles, and the controllers based on the law can achieve good economic performance of HESS.
(2) Considering traffic information in a controller is beneficial to the performance promotion of HESS.

In future works, the vehicle experiment for the comprehensive controller will be conducted.

Author Contributions: J.H. wrote the first draft of the manuscript, completed the offline optimization of dynamic programming, and developed the fuzzy logic controller considering traffic information. X.J. fitted the offline data and designed the adaptive rule-based controller. M.J. and Y.Z. provided insights and additional ideas on presentation. All of the authors revised and approved the manuscript.

Funding: This research received no external funding.

Acknowledgments: This work was supported by the Chongqing Natural Science Foundation (Project No. cstc2015jcyjA60005), the Fundamental Research Funds for the Central Universities (Project No. 106112016CDJXZ338825), and the National Key Research and Development Program of China (Project No. 2016YFB0101402). These projects offered all of the costs of this series of research. The authors appreciate for their supports on this research.

Conflicts of Interest: The authors declare no conflict of interest.

References

1. Jordán, J.; Palanca, J.; Val, E.D.; Julian, V.; Botti, V. A Multi-Agent System for the Dynamic Emplacement of Electric Vehicle Charging Stations. *Appl. Sci.* **2018**, *8*, 313. [CrossRef]
2. Gong, H.; Zou, Y.; Yang, Q.; Fan, J.; Sun, F. Generation of a driving cycle for battery electric vehicles: A case study of Beijing. *Energy* **2018**, *150*, 901–912. [CrossRef]
3. Cheng, L.; Wang, W.; Wei, S.; Lin, H.; Jia, Z. An Improved Energy Management Strategy for Hybrid Energy Storage System in Light Rail Vehicles. *Energies* **2018**, *11*, 423. [CrossRef]
4. Fu, Z.M.; Wang, B.; Zhou, P.G. An improved logic threshold approach of energy management for a power-split hybrid electric vehicle. In Proceedings of the International Conference on Advanced Mechatronic Systems, Zhengzhou, China, 29 August–2 September 2018; pp. 244–248.

5. Xiang, C.; Wang, Y.; Hu, S.; Wang, W. A New Topology and Control Strategy for a Hybrid Battery-Ultracapacitor Energy Storage System. *Energies* **2014**, *7*, 2874–2896. [CrossRef]
6. Wu, J.; Peng, J.; He, H.; Luo, J. Comparative Analysis on the Rule-based Control Strategy of Two Typical Hybrid Electric Vehicle Powertrain. *Energy Procedia* **2016**, *104*, 384–389. [CrossRef]
7. Wang, Y.; Wang, W.; Zhao, Y.; Yang, L.; Chen, W. A Fuzzy-Logic Power Management Strategy Based on Markov Random Prediction for Hybrid Energy Storage Systems. *Energies* **2016**, *9*, 25. [CrossRef]
8. Ferreira, A.A.; Pomilio, J.A.; Spiazzi, G.; Silva, L.D.A. Energy Management Fuzzy Logic Supervisory for Electric Vehicle Power Supplies System. *IEEE Trans. Power Electron.* **2008**, *23*, 107–115. [CrossRef]
9. Jaafar, A.; Akli, C.R.; Sareni, B.; Roboam, X.; Jeunesse, A. Sizing and Energy Management of a Hybrid Locomotive Based on Flywheel and Accumulators. *IEEE Trans. Veh. Technol.* **2009**, *58*, 3947–3958. [CrossRef]
10. Song, Z.; Hofmann, H.; Li, J.; Hou, J.; Han, X.; Ouyang, M. Energy management strategies comparison for electric vehicles with hybrid energy storage system. *Appl. Energy* **2014**, *134*, 321–331. [CrossRef]
11. Santucci, A.; Sorniotti, A.; Lekakou, C. Power split strategies for hybrid energy storage systems for vehicular applications. *J. Power Sources* **2014**, *258*, 395–407. [CrossRef]
12. Chen, B.C.; Wu, Y.Y.; Tsai, H.C. Design and analysis of power management strategy for range extended electric vehicle using dynamic programming. *Appl. Energy* **2014**, *113*, 1764–1774. [CrossRef]
13. Chen, S.Y.; Hung, Y.H.; Wu, C.H.; Huang, S.T. Optimal energy management of a hybrid electric powertrain system using improved particle swarm optimization. *Appl. Energy* **2015**, *160*, 132–145. [CrossRef]
14. Chen, Z.; Xiong, R.; Cao, J.; Lund, H.; Kaiser, M.J. Particle swarm optimization-based optimal power management of plug-in hybrid electric vehicles considering uncertain driving conditions. *Energy* **2016**, *96*, 197–208. [CrossRef]
15. Xiao, R.; Liu, B.; Shen, J.; Guo, N.; Yan, W.; Chen, Z. Comparisons of Energy Management Methods for a Parallel Plug-In Hybrid Electric Vehicle between the Convex Optimization and Dynamic Programming. *Appl. Sci.* **2018**, *8*, 218. [CrossRef]
16. Hu, X.; Moura, S.J.; Murgovski, N.; Bo, E.; Cao, D. Integrated Optimization of Battery Sizing, Charging, and Power Management in Plug-In Hybrid Electric Vehicles. *IEEE Trans. Control. Syst. Technol.* **2016**, *24*, 1036–1043. [CrossRef]
17. Godina, R.; Rodrigues, E.M.G.; Pouresmaeil, E.; Matias, J.C.O.; Catalão, J.P.S. Model Predictive Control Home Energy Management and Optimization Strategy with Demand Response. *Appl. Sci.* **2018**, *8*, 408. [CrossRef]
18. Zhou, F.; Xiao, F.; Chang, C.; Shao, Y.; Song, C. Adaptive Model Predictive Control-Based Energy Management for Semi-Active Hybrid Energy Storage Systems on Electric Vehicles. *Energies* **2017**, *10*, 1063. [CrossRef]
19. Zhang, S.; Xiong, R.; Sun, F. Model predictive control for power management in a plug-in hybrid electric vehicle with a hybrid energy storage system. *Appl. Energy* **2017**, *185*, 1654–1662. [CrossRef]
20. Lei, Z.; Qin, D.; Liu, Y.; Peng, Z.; Lu, L. Dynamic energy management for a novel hybrid electric system based on driving pattern recognition. *Appl. Math. Model.* **2017**, *45*, 940–954. [CrossRef]
21. Salmasi, F.R. Control Strategies for Hybrid Electric Vehicles: Evolution, Classification, Comparison, and Future Trends. *IEEE Trans. Veh. Technol.* **2007**, *56*, 2393–2404. [CrossRef]
22. He, H.; Guo, J.; Sun, C. Road Grade Prediction for Predictive Energy Management in Hybrid Electric Vehicles ☆. *Energy Procedia* **2017**, *105*, 2438–2444. [CrossRef]
23. Hovgard, M.; Jonsson, O.; Murgovski, N.; Sanfridson, M.; Fredriksson, J. Cooperative energy management of electrified vehicles on hilly roads. *Control. Eng. Pract.* **2018**, *73*, 66–78. [CrossRef]
24. Bouwman, K.R.; Pham, T.H.; Wilkins, S.; Hofman, T. Predictive Energy Management Strategy Including Traffic Flow Data for Hybrid Electric Vehicles. *IFAC-PapersOnLine* **2017**, *50*, 10046–10051. [CrossRef]
25. Song, Z.; Hofmann, H.; Li, J.; Han, X.; Zhang, X.; Ouyang, M. A comparison study of different semi-active hybrid energy storage system topologies for electric vehicles. *J. Power Sources* **2015**, *274*, 400–411. [CrossRef]
26. Wang, J.; Liu, P.; Hicks-Garner, J.; Sherman, E.; Soukiazian, S.; Verbrugge, M.; Tataria, H.; Musser, J.; Finamore, P. Cycle-life model for graphite-LiFePO$_4$ cells. *J. Power Sources* **2011**, *196*, 3942–3948. [CrossRef]
27. Luo, Y.; Wang, F.; Yu, H. Research on LiFePO$_4$ battery life model based on driving cycle. *Automobile Eng.* **2015**, *8*, 881–885.
28. Luo, Y.; Liu, X.; Liang, W. Design of hybrid energy storage system for electric vehicles to extend the life of lithium ion batteries. *J. South China Univ. Technol.* **2016**, *44*, 51–59.

29. Song, Z.; Hofmann, H.; Li, J.; Han, X.; Ouyang, M. Optimization for a hybrid energy storage system in electric vehicles using dynamic programing approach. *Appl. Energy* **2015**, *139*, 151–162. [CrossRef]
30. Introduction to Geographic Information Systems. Available online: https://www.mheducation.com/highered/product/introduction-geographic-information-systems-chang/M0078095131.html (accessed on 8 July 2018).
31. Research on highway route design system. Available online: http://www.cqvip.com/qk/93913x/201128/39195995.html (accessed on 8 July 2018).
32. Ding, F.; Wang, W.D.; Xiang, C.L.; He, W.; Qi, Y.L. Speed prediction and energy management for hybrid electric vehicles based on driving recognition. *Automob. Eng.* **2017**, *39*, 1223–1231.
33. Kanungo, T.; Mount, D.M.; Netanyahu, N.S.; Piatko, C.D.; Silverman, R.; Wu, A.Y. An efficient k-means clustering algorithm: analysis and implementation. *IEEE Trans. Pattern Anal. Mach. Intell.* **2002**, *24*, 881–892. [CrossRef]